Contactless Rotor Ground Fault Detection Method for Brushless Synchronous Machines Based on an AC/DC Rotating Current Sensor

Miguel A. Pardo-Vicente , José M. Guerrero , Carlos Antonio Platero * , And José A. Sánchez

Posted Date: 13 October 2023

doi: 10.20944/preprints202310.0818.v1

Keywords: Alternate Current; Direct Current; Rotor Fault Detection; Current Sensor

Article

Contactless Rotor Ground Fault Detection Method for Brushless Synchronous Machines Based on an AC/DC Rotating Current Sensor

Miguel A. Pardo-Vicente [1], José M. Guerrero [2], Carlos A. Platero [3,*] and José A. Sánchez [1]

[1] Hydraulic, Energy and Environmental Engineering Department, Universidad Politécnica de Madrid, 28040, Madrid, Spain; ma.pardo@alumnos.upm.es, joseangel.sanchez@upm.es

[2] Electric Department, Universidad del País Vasco / Euskal Herriko Unibertsitatea, 48013, Bilbao, Spain; josemanuel.guerrerog@ehu.eus

[*] Automatic, Electric and Electronic Engineering and Industrial Computing Department, Universidad Politécnica de Madrid, 28003, Madrid, Spain.

[*] Correspondence: carlosantonio.platero@upm.es

Abstract: Brushless Synchronous Machines (BSM) are replacing conventional synchronous machines with static excitation in generation facilities due to the absence of sparking and lower maintenance. However, this excitation system makes challenging measuring electric parameters in the rotor. This fact highly difficult the detection of ground faults, which are the most common type of electrical fault in electric machines. In this paper, a ground fault detection method for BSM is proposed. It is based on an inductive AC/DC rotating current sensor installed in the shaft. In case of a ground fault in the rotating parts of the BSM, a fault current will flow through the rotor's sensor, inducing voltage in its stator. Analyzing the frequency components of the induced voltage the detection of a ground fault in the rotating elements is possible. The ground faults detection method proposed covers the whole rotor and discern between DC and AC sides. To corroborate the detection method, experimental tests have been performed using a prototype of this sensor connected to laboratory synchronous machines achieving satisfactory results.

Keywords: alternate current; direct current; rotor fault detection; current sensor

1. Introduction

Brushless synchronous machines (BSM) are widely implemented in electricity generation power plants [1,2], high efficiency processes [3] and systems where sparking should not happen, such as in aircraft applications [4,5]. The absence of brushes to feed the excitation winding of the main synchronous machine (SM) implies a second machine, called exciter. The exciter is a synchronous machine whose armature winding is in its rotor and its field winding is in its stator. The stator of the exciter is fed from a static excitation system. The exciter armature winding is connected to the field winding of the main SM through a rotating rectifier. Therefore, the exciter armature currents are transformed into DC for the excitation of the main SM. The differences between a BSM and a static excitation SM can be observed in Figure 1.

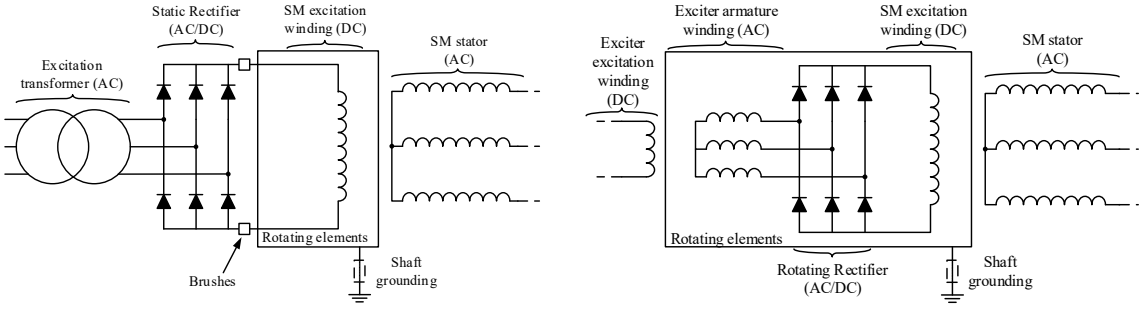

 doi:10.20944/preprints202310.0818.v1

Figure 1. Electrical schemes of synchronous machines [(a): Static excitation SM electrical scheme; (b): BSM electrical scheme].

Despite BSM high efficiency and large operating lifetime, the fault diagnosis in these machines is challenging. This is due to the lack of rotor electrical measurements, as there are not many ~~numerous~~ sensors suitable for rotating operation. In a previous research work [6], the authors developed an AC/DC current sensor based on an inductive coupling between two windings, placed in stator and rotor, respectively.

The development of novel techniques for current measurement is a very active research topic. For example, in the case of load monitoring [7] where the current wave form is very important, in case of distortion in power systems [8] or even in case of lightning current measurement [9] by optical sensors.

The absence of brushes in BSM does not allow getting measurements of rotor electrical magnitudes. Rotor faults account for around 10% of total machine electrical and mechanical faults [10] and their detection in BSM is not an easy task.

Different type of faults can appear in the rotor of BSM, such as diode faults [11], inter-turns faults or phase-to-phase faults [2], broken wires or open phase faults [12] and ground faults (GF). Ground faults, mainly caused by insulation aging, are the most common type of faults in power systems [13], and one of the most commons in electric machines. In ungrounded systems, a first GF does not provoke significant alterations in the circuit. However, if this fault is not repaired and a second one occurs, a large fault current will flow through the grounded points causing severe damages in the machine. Therefore, protecting the machines against ground faults is very important.

On the one hand, machine stator protection against GF can be achieved installing differential relays [14]. However, this application is effective only for low impedance grounding. It is a common practice, in power generation applications, the limitation of ground fault currents using high impedance grounding. Therefore, the differential relays do not see GF. In this case, zero sequence voltage protections are recommended [15]. Other possibility is injecting an AC current between ground and the stator winding [16,17], which also allows the fault location. But these last methods are complex to implement. As an additional solution, 100% earth-stator protections can be used combining a neutral overvoltage protection with a third harmonic minimum voltage protection [18,19].

On the other hand, the field windings of SM with static excitation can be protected using active methods that inject an AC or DC current between terminals of the winding and ground [20]. The injection device can easily be placed in the static side of the excitation system. However, the shaft must be connected to ground through an additional brush or a cooper braid. In this case, the fault current will flow through the braid to the AC or DC voltage injection source and the current can be measured. In [21,22], the AC or DC injection source is not required, as the secondary of the excitation system feeding transformer is grounded through a high value resistor that limits the maximum fault current. With the same phenomenon, the fault current flows through the grounding resistor. If the voltage between terminals of this resistor is different from zero, it implies a GF in the excitation system. The fault current path of this system can be observed in Figure 2a. Other off-line detection methods can be also implemented once the machine has previously tripped or during maintenance, for example, frequency response analysis (FRA) methods. However, these FRA methods need, in most cases, to extract the rotor to perform the diagnosis [23].

Preprints (www.preprints.org) | NOT PEER-REVIEWED | Posted: 13 October 2023 doi:10.20944/preprints202310.0818.v1

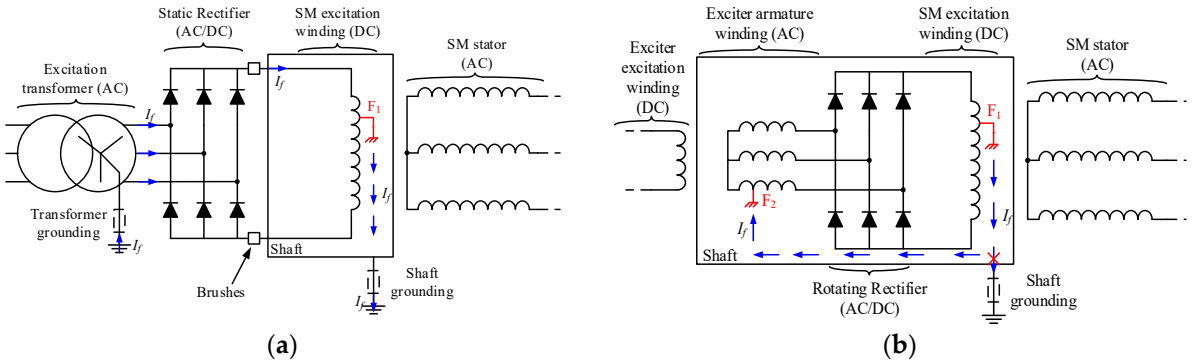

Figure 2. Examples of ground fault current paths for different types of synchronous machines [(a): Static excitation SM ground fault current path through excitation transformer grounding impedance; (b): BSM ground fault current path, F1: first ground fault, F2: second ground fault].

Nevertheless, in brushless applications, even if the shaft is grounded, the fault current will not flow outside of the rotor as the returning path is opened between the groundings of the static parts (exciter excitation winding) and the rotating parts. Consequently, the fault current will not flow outside of the rotor and the shaft. This fact makes challenging the GF detection with relays placed out of the rotor and consequently most of the BSM protection relays are based on the interturn or rotor phase short-circuit faults, i.e., the first GF is not detected, and the protection relays wait to a second GF that provokes a more severe situation (see Figure 2b). Common techniques to detect the short circuits in the rotor of BSM are airgap flux monitoring [12,24], stray flux monitoring [25,26] or static electrical parameters analysis [2,12]. In case of flux monitoring, airgap flux techniques are more invasive than stray flux ones, but they provide higher precision when measuring. The interturn faults are detected due to little asymmetries in the flux measurements because the field winding shorted is able to create less flux than healthy ones [24,26]. In [2], the state of the exciter armature winding is monitored based on the relative percentage of first and second harmonics of the stator field current compared with its DC component. If this percentage is over a certain threshold, it implies the existence of a fault in the rotor. The study presented in [12] also proposes the stator current measurement, since a failure in the rotor provokes alterations in the airgap flux which, at the same time, are reflected in the output currents. Finally, [26] analyzes the transient exciter and SM stator currents at the same time that the airgap and stray flux. Attending to the time-frequency plot of each parameter, field winding inter-turns faults of the main machine can be diagnosed.

In this paper, the monitoring of rotors in brushless synchronous machines against ground faults, based on the use of an AC/DC rotating current sensor, is proposed. Consequently, the problem of waiting until a short-circuit is produced by 2 GFs is avoided and an early diagnostic of the BSM can be achieved. The method is based on measuring the leakage current through the neutral of the power supply and ground in case of fault.

A previous method was developed for static excitation systems [21]. In that case, the neutral of the excitation transformer was grounded by a limiting resistor (see Figure 2a). In case of a fault in the AC side of the excitation, the leakage current frequency corresponds to the grid frequency (f_1). On the other hand, if the fault is in the rotor, the frequency is three times the grid frequency ($3 \times f_1$) [22].

Afterwards, this previous method was adapted and used for brushless excitation systems [27]. In this case, the armature winding of the exciter should be in star connection with neutral. Also, it was necessary to install an auxiliary slip ring and brush on the neutral of the exciter. A limiting resistor was connected from the auxiliary brush to ground in order to measure the leakage current.

To eliminate the auxiliary slip ring and brush, a rotating AC/DC current sensor was previously developed. The sensor has two windings: rotor and stator. The induced voltage in the sensor's stator winding is proportional to the current flowing through the sensor rotor winding. The sensor was designed and tested by injecting AC and DC currents in order to obtain the V/mA ratio [6]. The proposed sensor was granted a Spanish patent [28].

Preprints (www.preprints.org) | NOT PEER-REVIEWED | Posted: 13 October 2023 doi:10.20944/preprints202310.0818.v1

The main contribution of this paper is the validation of the complete system, brushless synchronous machine and rotating AC/DC current sensor, by experimental tests in healthy and faulty conditions. Despite the fact that there are several factors that affect the operation of the system such as the impedances of the sensor for different frequencies, rotor capacities to ground or electromagnetic noise, the results have been satisfactory.

The advantages of the proposed method are mainly three:

- It allows the detection of a first ground fault in BSM before a short-circuit appears, avoiding high damages in the machine and providing an early diagnostic of the machine.
- It does not need any brush to measure the ground fault current in the rotor.
- It can discern if the fault is taking place in the armature winding of the exciter or in the field winding of the main SM attending to the frequency components of the sensor's measured voltage.

Afterwards, the paper is written as follows: Section II explains in detail the method operating principles and sensor characteristics. Then, Section III describes the experimental setup and Section IV shows the results gotten. Section V discuss these results, and finally, Section VI concludes the paper highlighting the main ideas of the manuscript.

2. Operation Principles of the Rotor Ground Fault Detection Method

The proposed method requires a rotating AC/DC current sensor coupled in the rotating shaft of the main BSM and the exciter. The current sensor is able to measure rotor AC and DC currents analyzing the voltage induced in its stator. This section is focused on two parts, a brief description of the sensor and then, the description of the detection method.

2.1. Inductive AC/DC rotating current sensor brief description

This subsection briefly describes the sensor which was previously developed by the authors. A detailed description of its design, operation, accuracy and performance can be found in [6]. The sensor has a rotating part coupled to the rotating shaft of the machine that will be diagnosed. The reliability of the sensor is similar to that of any rotating machine and its cost is negligible compared to the cost of a large brushless generator. It has two windings in series conforming a pair of poles. The stator has also two windings connected in series located only in a concentrated zone. The sensor's radial section can be seen in Figure 3.

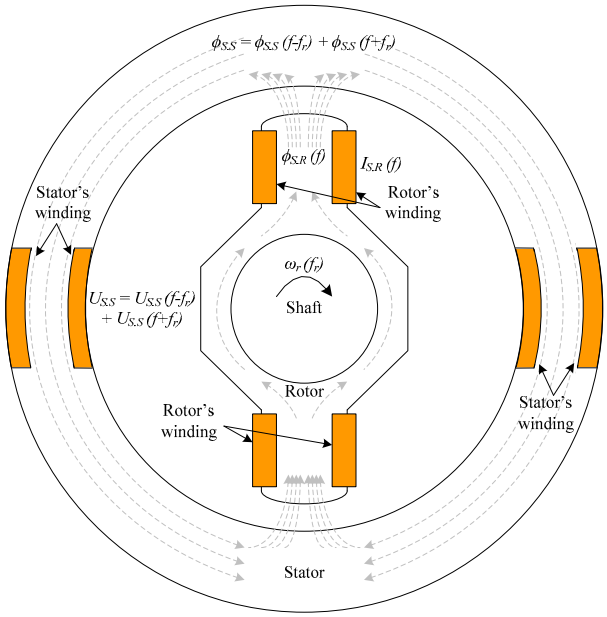

Figure 3. Current sensor coupled in the BSM shaft for the proposed contactless online ground fault detection.

Preprints (www.preprints.org) | NOT PEER-REVIEWED | Posted: 13 October 2023 doi:10.20944/preprints202310.0818.v1

In Figure 3, theorical fluxes are also plotted. First, the winding placed in the rotor measures a certain current $I_{S.R}$ with a frequency, f. This current will generate a flux, $\phi_{S.R}$ in the rotor of the sensor with the same frequency of this $I_{S.R}$ current. Following the magnetic circuit, $\phi_{S.R}$ pass through the airgap to the stator of the sensor. According to the Leblanc theorem, the flux is decomposed in two components: one with the frequency of $\phi_{S.R}$ plus the rotor's frequency ($f + f_r$) and the other with the frequency of $\phi_{S.R}$ minus the rotor's frequency ($f - f_r$). According to (1), the flux in the stator, $\phi_{S.S}$, is then:

$$\phi_{S.S} = \phi_{S.S}(f + f_r) + \phi_{S.S}(f - f_r) \quad (1)$$

Afterwards, the voltage in the stator winding of the sensor, U_S, can be monitored in real time, indirectly measuring the flux variations as:

$$U_S = N \cdot \left\{ \frac{d}{dt}[\phi_{S.S}(f + f_r)] + \frac{d}{dt}[\phi_{S.S}(f - f_r)] \right\} \quad (2)$$

where U_S will have the same frequency components than $\phi_{S.S}$. From (2), it can be seen that the voltage is proportional to the number of turns of the sensor stator winding. Therefore, as resolution increases with increasing voltage, it increases with increasing stator winding turns.

2.2. Ground fault detection method description

Once being able to measure the current in the rotor, indirectly by the analysis of the voltage induced in the sensor's stator, the GF detection method for BSM is carried out by installing the sensor according to Figure 4. In this figure, the neutral of the armature winding is connected in series with one terminal of the sensor's rotor. The other terminal is connected directly to the shaft. If needed, a resistive current limiter, R_{gnd}, can be connected between the other rotor terminal and the shaft.

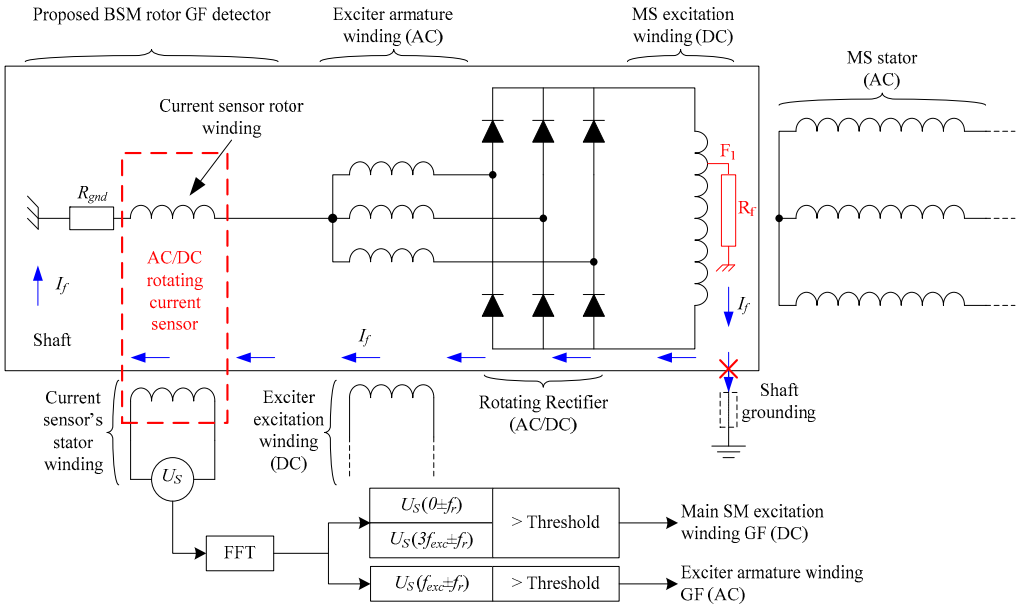

Figure 4. Proposed ground fault detection method for BSM based on a rotating current sensor connected between the neutral of the armature winding of the exciter and the shaft's chassis.

With this configuration, ground faults can be detected in the whole rotating elements, i.e., in the armature windings of the exciter (AC side) or in the field winding of the main machine (DC side).

In both cases, even if the shaft is grounded, the fault current path is closed inside the shaft and also limited by R_{gnd} to low values. Furthermore, the fault current, I_f, will be measured in the rotor's sensor ($I_{S.R} = I_f$).

Preprints (www.preprints.org) | NOT PEER-REVIEWED | Posted: 13 October 2023 doi:10.20944/preprints202310.0818.v1

2.2.1. AC Side: Armature winding of the exciter GF detection

On one hand, for a fault in the armature winding of the exciter, the fault current will have the frequency of the exciter AC side, which depends on the shaft rotating frequency and the number of pole pairs of the exciter machine. Therefore, $I_{R.S}$ will have the frequency of the exciter, f_{exc}, and also the rotor's flux, $\phi_{S.R}$. However, as explained before, due to the Leblanc theorem, U_S will measure other harmonic components, that in this case correspond with frequencies: $f_{exc} + f_r$ and $f_{exc} - f_r$.

2.2.2. AC Side: Armature winding of the exciter GF detection

On the other hand, for faults in the main machine field winding (an example can be seen in Figure 4), the I_f has mainly a DC and a $3 \cdot f_{exc}$ components. The DC component depends on the fault position and the $3 \cdot f_{exc}$ component depends on the fault resistance [22]. The DC flux induces voltages, at the rotor frequency. And the $3 \cdot f_{exc}$ component induces $3 \cdot f_{exc} + f_r$ and $3 \cdot f_{exc} - f_r$ in the stator of the current sensor. In this research work, a simple voltage threshold is proposed for detection purposes. However, a more complex analysis will be performed in future research work with the representative harmonics of U_S obtained by a Fast Fourier Transform (FFT).

Additionally, as the current sensor can be connected to the shaft with a high value R_{gnd}, the current is limited and the BSM does not have damages even in case of operation with ground fault. This fact allows to acquire a huge number of U_S wave cycles to improve the FFT process without damaging the machine.

3. Experimental Setup

The experimental setup comprises three machines as shown in the Figure 5. A special brushless synchronous machine (1) has been used. This synchronous machine is driven by an asynchronous motor (2). The brushless synchronous machine has a set of brushes and slip rings (3) connected to several points of the machine rotor. These points can be seen schematically in Figure 6. Therefore, it is possible to perform several internal faults and also to connect the neutral of the exciter to the rotating current sensor (4). The rotor winding of the rotating current sensor is grounded through a 5 kΩ limiting resistor, R_{gnd}. This resistor limits the fault current to a low enough value that does not damage the equipment. The internal faults are performed by the use of a variable resistor (5), configurable from 0 Ω to 5 kΩ (R_f = [0%,100%] of R_{gnd}). Also, the field winding of the exciter is fed by an adjustable voltage source (6). Finally, the sensor induced voltage is recorded by a FLUKE 196B oscilloscope (7), where an FFT is performed. The main characteristics of the experimental setup (main machine, exciter and sensor) are collected in Appendix A.

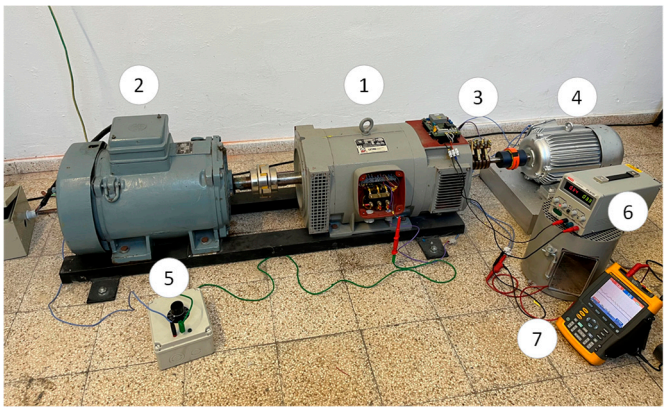

Figure 5. Experimental setup [(1): brushless synchronous machine; (2): induction motor; (3): brushes and slip rings; (4): rotating current sensor; (5): variable fault resistance; (6): adjustable voltage source; (7): oscilloscope].

Preprints (www.preprints.org) | NOT PEER-REVIEWED | Posted: 13 October 2023 doi:10.20944/preprints202310.0818.v1

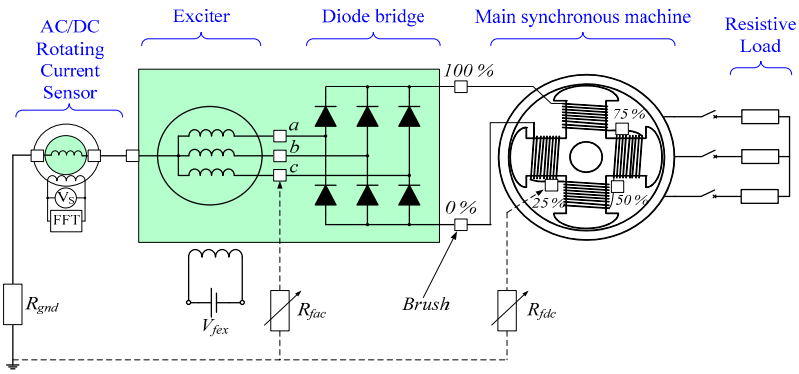

Figure 6. Experimental setup: simplified electrical diagram.

The sensor has been coupled to the shaft of the BSM through a flexible coupling. Both machines' shafts were aligned adjusting the position of the sensor with shims. The slip rings of the sensor have been connected to the slip rings of the BSM as shown in the electrical scheme of the experimental setup (Figure 6). Furthermore, the rotating current sensor geometry can be seen in Figure 7.

Figure 7. AC/DC rotating current sensor during manufacturing.

Regarding to the different operation frequencies, the main machine has 2 pair of poles, which implies that the shaft rotates at f_r = 25 Hz. However, the exciter has 6 pair of poles, which indicates that the currents flowing through the armature winding have a frequency of f_{exc} = 150 Hz.

4. Experimental Results

Numerous experimental tests have been performed in the experimental setup to corroborate the operation of the proposed ground fault detection methodology.

4.1. Healthy conditions tests

The first set of tests have been in healthy conditions. For this purpose, the main machine has been operated firstly at no-load conditions and then feeding a resistive load. The no-load test has been accomplished at rated voltage. Afterward, the resistive load has been connected to the stator of the main machine. As the resistive load is not adjustable, the excitation current of the exciter, I_{exc}, has been modified to vary the current supplied by the main machine armature. Consequently, the armature voltage changes accordingly.

As it can be clearly observed in Table 1, the induced voltages in the stator of the current sensor are almost constant and below 0.360 V for any operating condition. This happens because the current that returns through the neutral of the exciter is negligible. Only parasitic capacitive currents would

Preprints (www.preprints.org) | NOT PEER-REVIEWED | Posted: 13 October 2023 doi:10.20944/preprints202310.0818.v1

flow through the sensor. Then, the detection method is not altered due to load changes, which is a clear advantage.

Table 1. Healthy conditions experimental test results.

Operation Conditions			Current Sensor Induced Voltage U_S [V]							
I_{exc} [A]	V_{stator} [V]	I_{stator} [A]	25 [Hz]	50 [Hz]	75 [Hz]	100 [Hz]	125 [Hz]	425 [Hz]	475 [Hz]	RMS [V]
0.33	384	0.0	0.220	0.005	0.182	0.012	0.125	0.074	0.049	0.348
0.35	274	5.9	0.210	0.005	0.174	0.014	0.109	0.067	0.048	0.338
0.40	296	6.4	0.210	0.007	0.171	0.006	0.101	0.072	0.060	0.337
0.45	320	6.8	0.206	0.018	0.169	0.012	0.103	0.074	0.060	0.340
0.50	340	7.3	0.211	0.001	0.173	0.001	0.105	0.074	0.070	0.347
0.55	362	7.7	0.213	0.003	0.183	0.003	0.106	0.080	0.072	0.356
0.60	382	8.1	0.204	0.020	0.160	0.024	0.097	0.057	0.045	0.315

4.2. Rotor DC side ground faults: Main machine excitation winding

After verifying that the current sensor is not affected by load changes during healthy operation, the first ground faults were implemented in the field winding of the main machine (see F1 position in Figure 4). The fault resistance R_f has been varied from 5 kΩ to 0 kΩ to emulate different fault severities. Moreover, the faults have been located at the 0%, 25%, 50 %, 75 % and 100% of the field winding length. The negative terminal and the positive terminal of the winding corresponds to 0% and 100%, respectively (See Figure 6).

The root mean square (RMS) values of the sensor induced voltage, U_S, are displayed in Figure 8 at no-load conditions. The induced voltage increases as the fault resistance decreases. In case of R_f = 5 kΩ faults, the voltages in the armature winding of the sensor are between 0.82 V and 1.52 V, meanwhile, for zero-resistance faults the values increase considerably, between 1.90 V and 17 V. Therefore, a ground fault can be easily detected as the voltage increases almost by three times in the worst case (R_f = 5 kΩ). However, the faults in the midpoint of the windings apparently induce less voltage than faults in the ends of the winding.

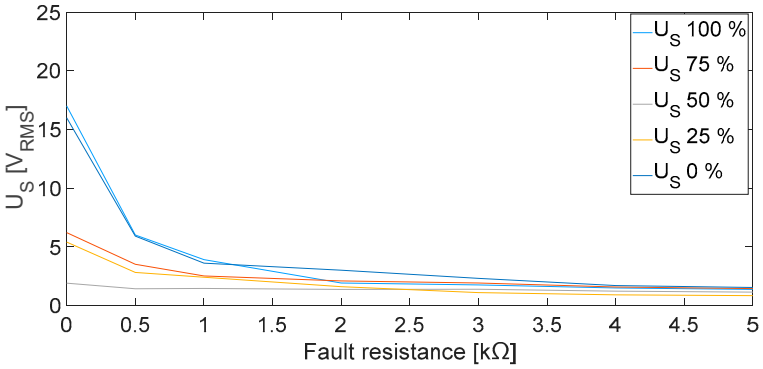

Figure 8. Sensor induced voltage, U_S , RMS values for ground faults in the field winding of the main machine at no load conditions [Fault positions 0, 25, 50, 75 and 100%].

The tests have been repeated with different armature currents changing the resistive load. The results are like those at no load. In Figure 9, the results, corresponding to an armature current of 8.1 A at rated voltage, are presented as an example. The induced voltage increases as the fault severity level increases. A 5 kΩ fault can be easily detected, as the induced voltage increases between 1.16 V and 1.79 V.

Preprints (www.preprints.org) | NOT PEER-REVIEWED | Posted: 13 October 2023 doi:10.20944/preprints202310.0818.v1

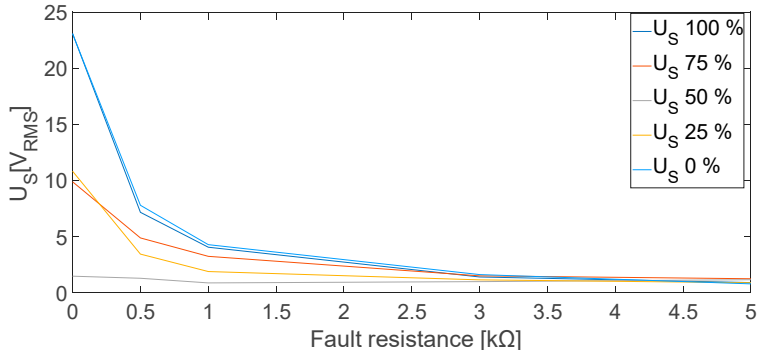

Figure 9. Sensor induced voltage, U_S , RMS values for ground faults in the field winding of the main machine at rated voltage on load conditions [Fault positions 0, 25, 50, 75 and 100%, I_{Load} = 8.1 A].

As an example, Figure 10a collects a 200 ms time domain measurement of the induced voltage in the sensor. The fault current that circulates through its rotor windings is mostly DC because the fault has been performed in the 0 % of the main machine exciter winding with R_f = 0 Ω. Therefore, the induced voltage will present narrow peaks due to the built sensor characteristics.

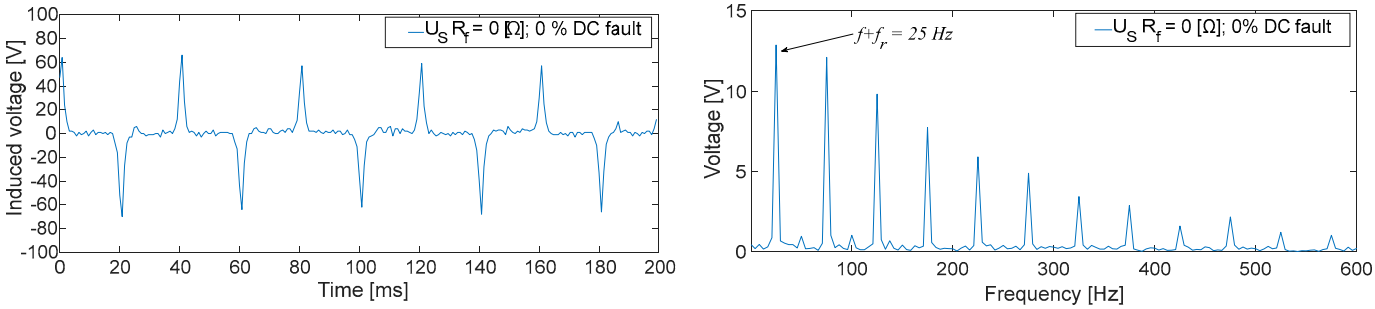

(**a**) (**b**)

Figure 10. U_S measurements corresponding to a ground fault in the field winding of the main machine at no-load conditions [Fault position: 0%; R_f = 0 [Ω]; (a): time domain; (b) frequency domain].

In this case, observing Figure 10b, the fundamental frequency when the FFT is performed is 25 Hz. It corresponds with the fault current frequency added to the rotating frequency ($f + f_r$).

4.3. Rotor AC side ground faults: Armature exciter winding

Furthermore, different ground faults have been accomplished in the AC side of the rotor circuit, corresponding to the armature windings of the exciter. This type of faults implies fault currents with 150 Hz frequency, i.e., the frequency of the induced currents in the armature windings of the exciter. Then, the frequencies induced in the stator of the sensor are $f - f_r$ = 125 Hz and $f + f_r$ = 175 Hz, as it can be seen in Figure 11. This figure shows an example of AC fault with R_f = 1 kΩ.

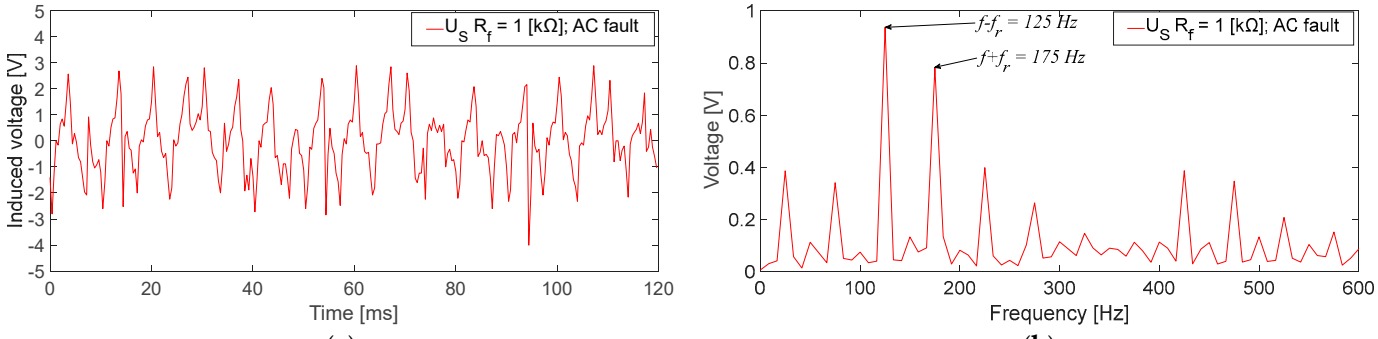

(**a**) (**b**)

Preprints (www.preprints.org) | NOT PEER-REVIEWED | Posted: 13 October 2023 doi:10.20944/preprints202310.0818.v1

Figure 11. U_S measurement for a ground fault in the armature winding of the exciter for no-load conditions [R_f = 1 kΩ; (a): time domain; (b) frequency domain].

Additionally, the results of AC side fault tests with different R_f are shown in Figure 12. The AC side faults can be detected as the RMS voltage increase from 0.36 V (healthy state) to 0.80 V (an increase of 222.3 % in the RMS value for the R_f = 5 kΩ case).

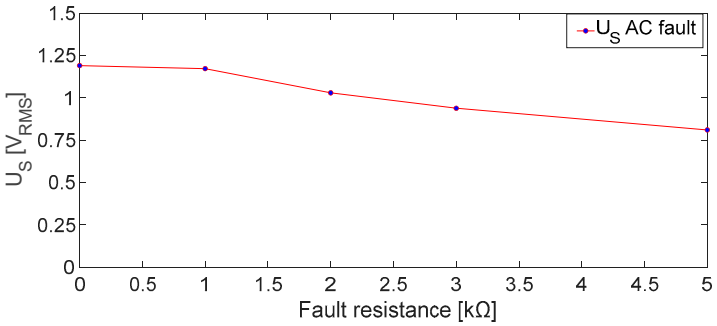

Figure 12. Sensor induced voltage (RMS), U_S, for ground faults in the armature winding of the exciter machine at no-load conditions.

5. Discussion

Based on the experimental results shown in the previous section, several remarks should be done.

First of all, it must be highlighted that the results at healthy conditions are not affected by load changes. However, U_S measured in the stator of the current sensor was not null. It is because, even with no ground fault, parasitic currents will flow through R_{gnd}. The maximum U_S value achieved was 0.356 V_{RMS}.

On the other hand, thanks to the high value of R_{gnd}, the leakage current is limited to 10 mA allowing the continuous operation during a first ground fault. Two types of faults have been performed: in the field winding of the main machine and in the armature winding of the exciter.

Faults in the excitation winding of the main machine (DC faults) presented a higher peak in the FFT of U_S in the 25 Hz harmonic. This harmonic corresponds to the DC component added to the rotor frequency. On one hand, the effect of position was explored observing that faults in the midpoint of the winding presented considerably lower RMS values than faults in the terminals of the winding. This is due to the system symmetry [18]. On the other hand, the fault resistance change was explored up to 100% of the value of R_{gnd}. Observing Figure 8, when R_f is higher (lower fault severity), sensor stator voltage decreases. The behavior is similar to a voltage divider between R_{gnd} and R_f. Analogous results have been achieved in other works for different R_f faults [29]. Other remark should be focused on the rectifier commutation frequency $3 \cdot f_{exc}$ = 450 Hz. According to Section II, the frequencies 425 Hz and 475 Hz were expected to appear when performing faults in the DC side, as the voltage ripple should be reflected in the fault current. However, those components reach low values. The explanation to this fact is that the inductive sensor actuates as a low frequency filter, adding impedance to the fault circuit path in higher frequencies. Therefore, the fault current becomes even more limited and, as a consequence, the induced voltage in the stator becomes lower. Despite of this filtering effect, faults in the midpoint of the winding can be observed thanks to the homopolar currents (450 Hz) returning through R_{gnd} and the current sensor. The lowest RMS value of U_S in the DC cases is 0.82 V, which means more than twice the value measured during healthy conditions.

Faults in the armature winding of the exciter (AC side) presented U_S higher harmonics at 125 Hz and 175 Hz, which mainly correspond to 150 Hz (armature current frequencies) ± 25 Hz (rotating frequency), according to the Leblanc theorem. In this case, only the fault resistance behavior was analyzed as in the experimental setup no intermediate positions could have been accessed without damaging the equipment's insulation. As seen in Figure 11, the RMS values are considerably lower than for DC faults. It is due to the filtering effects of the sensor. As previously commented, now the

 doi:10.20944/preprints202310.0818.v1

fault currents are mainly of 150 Hz instead of 0 Hz, then, the inductance of the sensor limits even more the fault current. In any case, the lowest U_S RMS value, corresponding to a R_f = 5 kΩ fault, is 0.80 V. Again, this value is greater than two times the value measured in healthy conditions.

Thus, it can be stated that the detection of ground faults in the rotor of brushless synchronous machines can be performed by installing a rotating current sensor between the neutral of the armature current winding and the rotor's shaft, and analyzing the frequency spectrum of its induced voltage.

6. Conclusions

Rotor measurements are difficult in brushless machines. This makes considerably difficult the protection and monitoring of the internal rotor parts. This paper has proposed a ground fault detection method for the rotor of brushless synchronous machines based on using an AC/DC rotating current sensor.

The method proposes the coupling of a rotating AC/DC current sensor between the neutral of the exciter armature winding and the shaft in series with a resistive current limiter. Thus, if a ground fault happens in the rotor, the fault circuit path is closed through the rotor shaft and passes through the sensor. This current induces a voltage in the sensor's stator where a frequency analysis is performed. Observing the induced voltage, the fault can be detected due to a large increase in its RMS value. Also, the zone can be discerned between armature winding faults (AC side) or main machine excitation winding faults (DC side). Where DC faults present their main harmonic at the rotor frequency, and AC faults present their main harmonics at the armature current frequency plus/minus the rotor frequency.

The proposed detection method has been checked through experimental tests obtaining results according to the previous formulated hypotheses.

In such manner, the method can detect faults up to 5 kΩ (maximum value tested in the laboratory), which is a normal setting of existing rotor ground fault protections. The measured RMS value increases more than twice compared with healthy conditions. In addition, the fault zone, AC or DC, can be discerned. However, its main weakness appears when analyzing higher frequencies, i.e., as the current sensor performs as a low-frequency filter, fault current sensitivity for high frequencies is reduced.

Based on the results obtained in this research, further works should be focused on two fields: On one hand, the fault location problem stays unsolved. On the other hand, modified current sensor designs could achieve better results and sensitivities.

7. Patents

The patent ES 2798048 B2 (4. 12. 2020) "Rotating Sensor for the Altern and/or Direct Current Measurement in Rotating Machines" was developed and is considered in the development of this research work.

Author Contributions: Authors contributions have been organized as follows: Conceptualization, MA.P. and CA.P.; methodology, CA.P. and JA.S; software, MA.P. and JM.G.; validation, MA.P., JM.G., and CA.P.; formal analysis, CA.P. and JA.S.; investigation, MA.P.; resources, MA.P.; writing—original draft preparation, MA.P.; writing—review and editing, JM.G., CA.P. and JA.S; visualization, JM.G.; supervision, JA.S.; funding acquisition, JA.S. All authors have read and agreed to the published version of the manuscript.

Funding: This research was funded by Universidad Politécnica de Madrid under grant number RP2304330031.

Institutional Review Board Statement: Not applicable.

Informed Consent Statement: Not applicable.

Data Availability Statement: Data will be available under request.

Conflicts of Interest: The authors declare no conflict of interest.

Preprints (www.preprints.org) | NOT PEER-REVIEWED | Posted: 13 October 2023 doi:10.20944/preprints202310.0818.v1

Appendix A

Table A1. Synchronous machine data.

Parameter	Magnitude	Units
Machine type	Brushless Synchronous Machine	
Rated power	12.5	kVA
Rated speed	1500	rpm
Rated voltage	400	V
Rated power factor	0.8	
Rated current	18	A
Phases	3	
Rated frequency	50	Hz
Isolation class	F	

Table A2. Exciter machine data.

Parameter	Magnitude	Units
Machine type	Synchronous brushless	
Rated speed	1500	rpm
Rated excitation voltage	15	V
Rated excitation current	1.5	A
No-load excitation voltage	4.25	V
No-load excitation current	0.5	A
Phases	3	
Number of poles	12	
Isolation class	F	

Table A3. Sensor data.

Parameter	Magnitude	Units
Machine type	Prototype sensor	
Number of field poles	2	
Number of armature poles	2	
Number of turns of field winding	1000	
Number of turns of armature winding	3000	
Wires section	0.096	mm^2
Rated speed	1500	rpm
Rotor diameter	122.5	mm
Air gap	0.5	mm

References

1. L. Hao, J. Chang, L. Hu, X. Wang, W. Zong and L. Gui. Analysis of the Interturn Short Circuits of Stator Field Windings in Multiphase Angular Brushless Exciter at Nuclear Power Plant. *IEEE Transactions on Energy Conversion*, **2019**, vol. 34, no. 4, pp. 2126-2136. https://doi.org/10.1109/TEC.2019.2937128.
2. L. Hao, J. Chen, L. He, X. Duan, P. He and G. Wang. Modeling, Analysis, and Identification of Armature Winding Interturn Fault in Multiphase Brushless Exciters. *IEEE Transactions on Power Electronics*, Jan. **2023**, vol. 38, no. 1, pp. 1119-1131. https://doi.org/10.1109/TPEL.2022.3200675.
3. Y. Yan, S. S. H. Bukhari and J. -S. Ro. Novel Hybrid Consequent-Pole Brushless Wound Rotor Synchronous Machine for Improving Torque Characteristics. *IEEE Access*, **2022**, vol. 10, pp. 35953-35964. https://doi.org/10.1109/ACCESS.2022.3163824.
4. Y. Juan, X. Haiyi and Y. Zhangang. An Active Control Excitation Method of Three-Stage Brushless Synchronous Starter/Generator in Electric Starting Mode for MEA. *IEEE Access*, **2021**,vol. 9, pp. 109763-109774. https://doi.org/10.1109/ACCESS.2021.3102049.

5. S. Zhu, Y. Hu, J. Li, C. Liu and K. Wang. Magnetic Field Analysis and Operating Characteristics of a Brushless Electrical Excitation Synchronous Generator With DC Excitation. *IEEE Transactions on Magnetics*, **2022**, vol. 58, no. 8, pp. 1-7. https://doi.org/10.1109/TMAG.2022.3148173.
6. M. A. Pardo-Vicente, C. A. Platero, J. Á. Sánchez-Fernández, and F. Blázquez. AC/DC Current Sensor for Rotating Applications. *Sensors*, 2020, vol. 20, no. 23, p. 6811. https://doi.org/10.3390/s20236811
7. Shareef, H.; Asna, M.; Errouissi, R.; Prasanthi, A. Rule-Based Non-Intrusive Load Monitoring Using Steady-State Current Waveform Features. Sensors 2023, 23(15), 6926; https://doi.org/10.3390/s23156926.
8. Zhong, C.; Zhang, Z.; Zhu, A.; Liang, B. An Adaptive Virtual Impedance Method for Grid-Connected Current Quality Improvement of a Single-Phase Virtual Synchronous Generator under Distorted Grid Voltage. Sensors 2023, 23(15), 6857; https://doi.org/10.3390/s23156857.
9. Ge, J.; Yin, Y.; Wang, W. Lightning Current Measurement Form and Arrangement Scheme of Transmission Line Based on Point-Type Optical Current Transducer. Sensors 2023, 23(17), 7467; https://doi.org/10.3390/s23177467.
10. K. N. Gyftakis and A. J. M. Cardoso. Reliable Detection of Stator Interturn Faults of Very Low Severity Level in Induction Motors. *IEEE Transactions on Industrial Electronics*, **2021**, vol. 68, no. 4, pp. 3475-3484. https://doi.org/10.1109/TIE.2020.2978710.
11. J. Pang, W. Liu, Z. Wei, C. Sun, N. Jiao and X. Han. Online Diode Fault Detection in Rotating Rectifier of the Brushless Synchronous Starter Generator. *IEEE Transactions on Industrial Informatics*, **2020**, vol. 16, no. 11, pp. 6943-6951. https://doi.org/10.1109/TII.2020.2974268.
12. H. J. Kim, M. F. Shaikh, S. B. Lee, C. A. Platero and T. Kim. Alternative Test Methods for Monitoring the Condition of Brushless Exciters in Synchronous Machines. *IEEE Transactions on Energy Conversion*, **2022**, vol. 37, no. 3, pp. 2009-2018. https://doi.org/10.1109/TEC.2022.3142238.
13. U. Snahzad, S. Kahrobaee, S. Asgarpoor. Protection of Distributed Generation: Challenges and Solutions. *Energy and Power Engineering*, 2017, vol. 9, no.10, pp. 614-653. https://doi.org/10.4236/epe.2017.910042.
14. N. Fischer, D. Finney and D. Taylor. How to determine the effectiveness of generator differential protection. In proceedings of the 2014 67th Annual Conference for Protective Relay Engineers, Texas, USA, 31 March – 3 April 2014, pp. 408-420.. https://doi.org/10.1109/CPRE.2014.6799018.
15. P. Pillai et al. Grounding and Ground Fault Protection of Multiple Generator Installations on Medium-Voltage Industrial and Commercial Power Systems-Part 3: Protection Methods Working Group Report. *IEEE Transactions on Industry Applications*, **2004**, vol. 40, no. 1, pp. 24–28. https://doi.org/10.1109/TIA.2003.821644.
16. N. Safari-Shad, R. Franklin, A. Negahdari, and H. A. Toliyat. Adaptive 100% injection-based generator stator ground fault protection with real-time fault location capability. *IEEE Transactions on Power Delivery*, **2018**, vol. 33, no. 5, pp. 2364–2372. https://doi.org/10.1109/TPWRD.2018.2802423.
17. W. Hartmann. Advanced Generator Ground Fault Protections — A Revisit with New Information. In proceedings of the 2019 72nd Conference for Protective Relay Engineers (CPRE), Texas, USA, 25 – 28 March 2019, pp. 1-23. https://doi.org/10.1109/CPRE.2019.8765867.
18. C. A. Platero, M. Redondo, M. Pardo and E. Rebollo. Novel adaptive 100% stator ground fault protection based on the third harmonic measurement. In proceedings of the 2016 XXII International Conference on Electrical Machines (ICEM), Lausanne, Switzerland, 4 – 7 September 2016, pp. 2300-2305. https://doi.org/10.1109/ICELMACH.2016.7732842.
19. K. Al Jaafari, A. Negahdari, H. A. Toliyat, N. Safari-Shad and R. Franklin. Modeling and Experimental Verification of a 100% Stator Ground Fault Protection Based on Adaptive Third-Harmonic Differential Voltage Scheme for Synchronous Generators. *IEEE Transactions on Industry Applications*, **2017**, vol. 53, no. 4, pp. 3379-3386. https://doi.org/10.1109/TIA.2017.2682165.
20. J. Qiao, X. Yin, Y. Wang, Q. Lu, L. Tan and L. Zhu. A Rotor Ground Fault Protection Method Based on Injection Principle for Variable Speed Pumped Storage Generator-Motor. IEEE Transactions on Power Delivery, **2023**, vol. 38, no. 2, pp. 1159-1168. https://doi.org/10.1109/TPWRD.2022.3209971.
21. C. A. P. Gaona, F. Blázquez, P. Frías and M. Redondo. A Novel Rotor Ground-Fault-Detection Technique for Synchronous Machines With Static Excitation. *IEEE Transactions on Energy Conversion*, **2010**, vol. 25, no. 4, pp. 965-973. https://doi.org/10.1109/TEC.2010.2040739.
22. C. A. Platero, F. Blázquez, P. Frías and M. Pardo. New On-Line Rotor Ground Fault Location Method for Synchronous Machines With Static Excitation. *IEEE Transactions on Energy Conversion*, **2011**, vol. 26, no. 2, pp. 572-580. https://doi.org/10.1109/TEC.2010.2095501.
23. C. M. Martín, J. M. Guerrero, P. Gómez Mourelo and C. A. Platero. Ground Faults Location in Poles of Synchronous Machines Through Frequency Response Analysis. *IEEE Transactions on Industry Applications*, **2022**, vol. 58, no. 1, pp. 113-122. https://doi.org/10.1109/TIA.2021.3122412.
24. M. F. Shaikh, H. -j. Kim, S. B. Lee and C. Lim. Online Airgap Flux Based Diagnosis of Rotor Eccentricity and Field Winding Turn Insulation Faults in Synchronous Generators. *IEEE Transactions on Energy Conversion*, **2022**, vol. 37, no. 1, pp. 359-366. https://doi.org/10.1109/TEC.2021.3092198.

25. P. Tian, J. Antonino-Daviu, C. A. Platero and L. Dunai. Detection of Field Winding Faults in Synchronous Motors via Analysis of Transient Stray Fluxes and Currents. IEEE Transactions on Energy Conversion, **2021**, vol. 36, no. 3, pp. 2330-2338. https://doi.org/10.1109/TEC.2020.3041643.
26. H. Ehya and A. Nysveen. Pattern Recognition of Interturn Short Circuit Fault in a Synchronous Generator Using Magnetic Flux. *IEEE Transactions on Industry Applications*, **2021**, vol. 57, no. 4, pp. 3573-3581. https://doi.org/10.1109/TIA.2021.3072881.
27. M. A. Pardo, K. Mahtani, C. A. Platero and J. A. Sánchez-Fernández. On-line Rotor Ground Fault Location Method for Brushless Synchronous Machines. *IEEE Transactions on Industry Applications*, **2023**, vol. 59, no. 3, pp. 3067-3076. https://doi.org/10.1109/TIA.2023.3248020.
28. M. A. Pardo-Vicente, C. A. Platero, F. Blázquez, J. A. Sánchez. Sensor Rotativo para Medida de Corriente Alterna y/o Corriente Continua en Máquinas Rotativas. Spanish Patent 2798048 B2, Dec. 4, 2020, Oficina Española de Patentes y Marcas, Madrid.
29. J. M. Guerrero, G. Navarro, C.A. Platero, P. Tian, F. Blazquez. A Novel Ground Fault Detection Method for Electric Vehicle Powertrains Based on a Grounding Resistor Voltage Analysis. *IEEE Transactions on Industry Applications*, 2020, vol. 56, no. 5, pp. 4934-4944. https://doi.org/10.1109/TIA.2020.3000965.